J. Fluid Mech. (2001), *vol.* 433, *pp.* 383–409. Printed in the United Kingdom

Experimental indications for Markov properties of small-scale turbulence

By CHRISTOPH RENNER[1], J. PEINKE[1] AND R. FRIEDRICH[2]

[1]Department of Physics, University of Oldenburg, D-26111 Oldenburg, Germany

[2]Institute of Theoretical Physics, University of Stuttgart, D-70550 Stuttgart, Germany

(Received 30 March 2000 and in revised form 25 October 2000)

We present a stochastic analysis of a data set consisting of 1.25×10^7 samples of the local velocity measured in the turbulent region of a round free jet. We find evidence that the statistics of the longitudinal velocity increment $v(r)$ can be described as a Markov process. This new approach to characterize small-scale turbulence leads to a Fokker–Planck equation for the r-evolution of the probability density function (p.d.f.) of $v(r)$. This equation for $p(v,r)$ is completely determined by two coefficients $D_1(v,r)$ and $D_2(v,r)$ (drift and diffusion coefficient, respectively). It is shown how these coefficients can be estimated directly from the experimental data without using any assumptions or models for the underlying stochastic process. The solutions of the resulting Fokker–Planck equation are compared with experimentally determined probability density functions. It is shown that the Fokker–Planck equation describes the measured p.d.f.(s) correctly, including intermittency effects. Furthermore, knowledge of the Fokker–Planck equation also allows the joint probability density of N increments on N different scales $p(v_1, r_1; \ldots; v_N, r_N)$ to be determined.

1. Introduction

The small-scale structure of fully developed turbulent flows is commonly believed to form an universal state which exhibits stationarity, homogeneity, and isotropy in a statistical sense, cf. Monin & Yaglom (1975) and Frisch (1995). This state is characterized by the existence of a flux of energy, which is injected into the fluid motion at large scales and is continuously transported towards smaller scales due to the inherent instability of vortices of a scale r towards perturbations on smaller scales. It is denoted the turbulent cascade and usually investigated by the statistics of the longitudinal velocity increments $v(r,t)$,

$$v(r,t) = \boldsymbol{e} \cdot [\boldsymbol{u}(\boldsymbol{x} + \boldsymbol{e}r, t) - \boldsymbol{u}(\boldsymbol{x}, t)], \tag{1.1}$$

where $\boldsymbol{e}$ denotes a unit vector with arbitrary direction and $\boldsymbol{x}$ denotes a reference point. For experimental reasons, the unit vector $\boldsymbol{e}$ is commonly chosen to point in the direction of the mean flow. Owing to homogeneity, the statistical properties of $v(r,t)$ are independent of the reference point $\boldsymbol{x}$. Owing to isotropy, the statistics are independent of the direction of the unit vector $\boldsymbol{e}$. Owing to stationarity, the moments $\langle v(r,t)^n \rangle = \langle v(r)^n \rangle$ are time independent.

It is of current interest to investigate whether the cascade exhibits self-similar behaviour in a statistical sense. The nth-order moment, $\langle v(r)^n \rangle$, also called the nth-

order structure function, should obey the following relationship:

$$\langle v(\alpha r)^n \rangle = \alpha^{\zeta_n} \langle v(r)^n \rangle. \tag{1.2}$$

The assumption of self-similarity (1.2) immediately implies scaling behaviour of the structure functions:

$$\langle v(r)^n \rangle = \left(\frac{r}{r_1} \right)^{\zeta_n} \langle v(r_1)^n \rangle. \tag{1.3}$$

Applying dimensional analysis, Kolmogorov (1941) suggested that the scaling indices ζ_n are linear functions of n

$$\zeta_n = \tfrac{1}{3} n. \tag{1.4}$$

Clearly, this is equivalent to a uniform rescaling of the velocity increments under the scale transformation (1.2). As suggested by Landau, see Landau & Lifschitz (1987), this uniform rescaling is violated due to the highly intermittent behaviour of the energy dissipation rate ϵ. The consequence is multifractal scaling behaviour,

$$\zeta_n = \tfrac{1}{3} n + \Delta_n, \tag{1.5}$$

where Δ_n is a nonlinear function of n. On the basis of a *refined similarity hypothesis* Kolmogorov (1962) and Obukhov (1962) suggested the so-called log-normal model leading to a definite form of the corrections Δ_n

$$\Delta_n = -\frac{\mu}{18} n(n-3). \tag{1.6}$$

Here, μ is the so-called intermittency parameter.

Since Kolmogorov's pioneering work, the problem of small-scale turbulence has attracted the attention of many researchers. Several models for the scaling exponent ζ_n have been proposed and numerous publications have been devoted to experimental verifications of the scaling behaviour. For a review of recent developments in this field, we refer to the paper by Sreenivasan & Antonia (1997) and the book by Frisch (1995).

An alternative way to characterize the turbulent cascade is to describe it by means of the probability density functions (p.d.f.) $p(v, r)$ of the velocity increment on scale r. Clearly, this approach is equivalent to the one via the structure functions (for given p.d.f.(s) $p(v, r)$, it is straightforward to calculate the moments $\langle v(r)^n \rangle$). The most significant characteristic of those p.d.f.(s) is their deviation from the Gaussian shape. This effect is closely related to the nonlinear correction in equation (1.5). Several parametrizations have been proposed to describe the shape of the p.d.f.(s), a well-known example being the approach by Castaing, Gagne & Hopfinger (1990).

Moreover, the description of the turbulent cascade by differential equations in the variables r and v for the probability densities $p(v, r)$ has become of interest, see Pedrizzetti & Novikov (1994). It has even been proposed that such equations can be derived from the Navier–Stokes equation, cf. Yakhot (1998) and Takahashi *et al.* (1999).

Furthermore, several recent investigations of turbulence point out that a more detailed characterization of the universal turbulent state might be achieved by taking into account the joint statistical properties of velocity increments on different scales r_i, see for instance Polyakov (1995), L'vov & Procaccia (1996), Chilla, Peinke & Castaing (1996), Nelkin & Stolovitzky (1996) and Pedrizzetti, Novikov & Praskovsky (1996).

Friedrich & Peinke (1997) demonstrated that the mathematics of Markov processes is a useful tool for experimental investigations of both the evolution of $p(v, r)$ in r and

the joint statistical properties of several increments on different scales. This method has been applied to the analysis of the local rate of energy dissipation in the papers of Naert, Friedrich & Peinke (1997), Marcq & Naert (1998) and Cleve & Greiner (2000). Results for the case of velocity increments of non-isotropic turbulence were reported by Lück, Peinke & Friedrich (1999) and Reisner *et al.* (1999). Extensions of this method to analyse complex spatio-temporal data of other fields such as surface roughness or financial data are given in the papers by Friedrich, Peinke & Renner (2000*a*), Friedrich *et al.* (1998*a*) and Friedrich *et al.* (2000*b*).

Based on the results by Friedrich & Peinke (1997), recent publications by Donkov, Donkov & Grancharov (1998), Davoudi & Tabar (1999), Dubrulle (2000) and Amblard & Brossier (1999) show the connection between common models of turbulence and the Markov property. The connection with fusion rules of N-increment moments as discussed by L'vov & Procaccia (1996) was pointed out by Davoudi & Tabar (2000).

Here, we extend the previous analysis by Friedrich & Peinke (1997) considerably. We show that it is possible to prove the existence of a Markov process experimentally and, furthermore, to extract the differential equation for this Markov process directly from the measured data. The procedure to obtain these results is presented in detail for one example data set obtained in a round free jet with Reynolds number $Re_\lambda = 190$. The corresponding experimental setup is described in § 2. In § 3 the standard data analysis is applied to our data. Section 4 is devoted to a brief summary of the theory of Markov processes and its application to the analysis of the statistics of the turbulent cascade. Section 5 contains the main results of our data analysis. In particular, we give evidence for the Markovian properties, provide estimates for Kramers–Moyal coefficients, and finally establish a Fokker–Planck equation which governs the scale dependence of the conditional probability density $p(v_1, r_1|v_2, r_2)$. We explicitly demonstrate that the solution of this equation accurately reproduces the empirically determined conditional probability densities. Owing to the Markovian property, we finally obtain a representation of the N-point statistics of the turbulent velocity cascade.

2. Experimental setup

The data were sampled by a hot-wire measurement in the central region of an air into air round free jet. The setup consists of a controlling unit for the flow rate, an inlet unit, the experimental chamber and the hot-wire anemometer, see figure 1.

The controlling unit (Bronkhorst EL-FLOW) for the flow rate allows us to vary the flow rate over five orders of magnitude with an accuracy of 1%. The air is supplied by a high-pressure reservoir (500 l at 200 bar) and pressure control units to diminish the pressure. Filtering during the compression of the air guarantees a constant quality (e.g. humidity) of the air.

The inlet unit consists of a calming area and a set of different grids settling the flow. The nozzle has a convex inner profile according to a suggestion by H. E. Fiedler and B. Blümel (Hermann-Föttinger-Institut Berlin, private communication) and an area contraction ratio of 22. The results presented here were obtained with a nozzle with an opening diameter of $D = 8$ mm. With the flow rates given above, the Reynolds number Re based on the diameter of the nozzle can be properly adjusted up to $Re_{max} = 3 \times 10^4$.

The closed experimental chamber is 2.5 m high and has a cross-section of 1 m^2. This size guarantees that a turbulent jet does not interact with the walls up to a distance

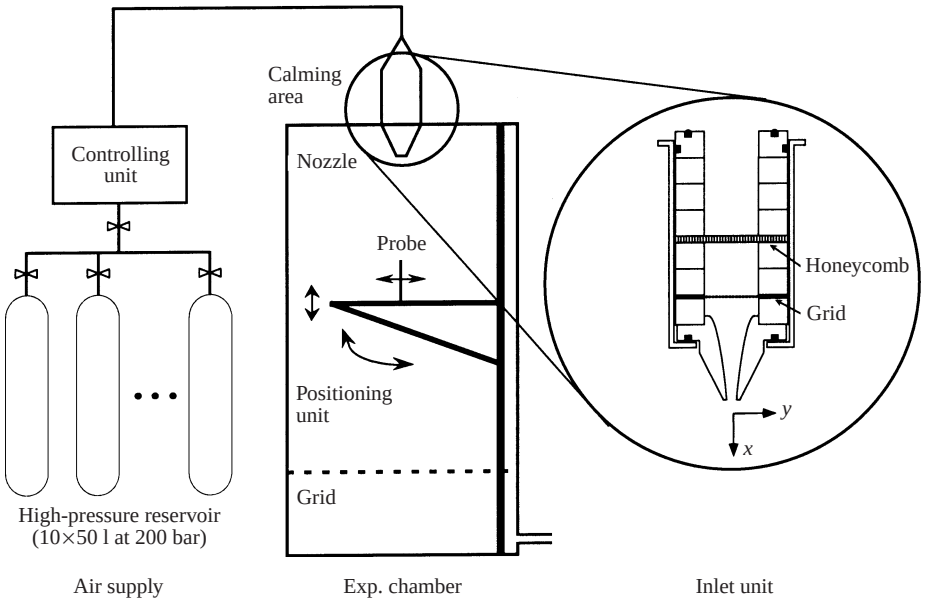

FIGURE 1. The experimental setup. The size of the experimental chamber is $2.5 \times 1 \times 1\,\mathrm{m}^3$. Details on the various components are given in the text.

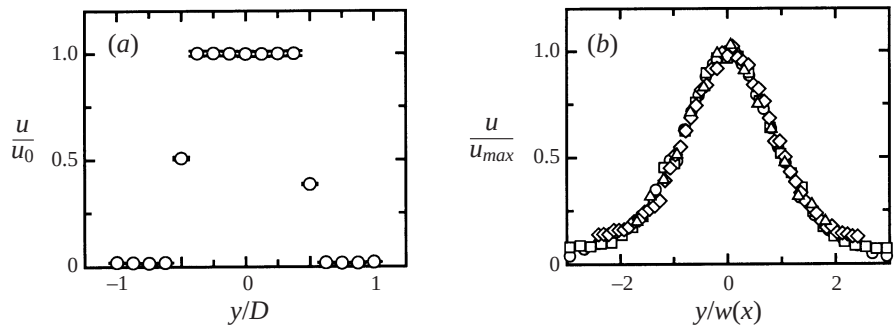

FIGURE 2. Radial velocity profiles of the free jet at different distances from the nozzle. (*a*) Profile in the near field of the jet. The streamwise distance from the nozzle is $x = 0.25D$, where D is the diameter of the nozzle ($D = 8\,\mathrm{mm}$). Velocities are given in units of u_0, the mean velocity at the nozzle ($u_0 = 27\,\mathrm{m\,s^{-1}}$), while y, the radial distance from the centre of the jet, is expressed in units of D (see figure 1 for a definition of the coordinates). (*b*) Several profiles in the far field. Circles: $x = 10D$, squares: $x = 50D$, diamonds: $x = 100D$, triangles: $x = 150D$. The profiles are normalized with respect to their respective maximal velocities $\langle u_x(x)\rangle_{max}$ and the widths $w(x)$, but have not been shifted in y.

of more than 150 nozzle diameters. In order to avoid interactions with the walls, the jet is relaminarized by a grid placed 1.5 m below the nozzle.

The time-resolved measurements of the local velocity in the direction of the mean flow were performed by means of hot-wire anemometry (Dantec frame 90N10). We used a single wire probe (Dantec 55P01) with a spatial resolution of 1.25 mm and a maximal time resolution of 30 kHz, verified by a square-wave test. A positioning unit enabled us to perform measurements at any position below the nozzle.

For an ideal free jet the flow close to the nozzle is expected to be non-turbulent and to have a top-hat profile. Furthermore, the radial mean velocity profiles in the far field (at a distance of more than $10D$ from the nozzle) are expected to have a self-similar shape, cf. Rajaratnam (1976).

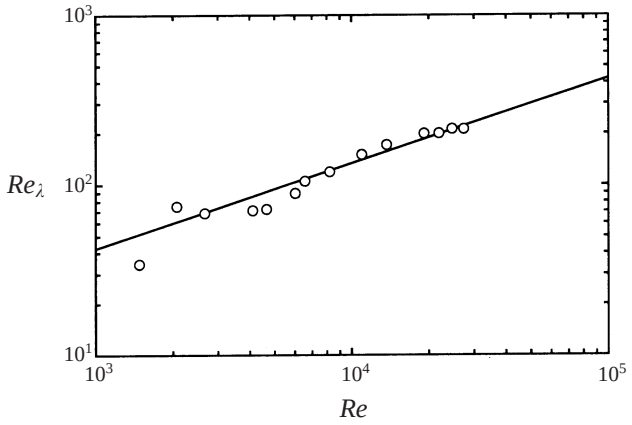

FIGURE 3. The Taylor Reynolds number Re_λ as a function of the nozzle-based Reynolds number Re. A fit to the experimental data (open circles) according to $Re_\lambda = c\sqrt{Re}$ (straight line) yields $c = 1.34 \pm 0.03$.

At a distance of $0.25D$ from the nozzle, measurements show that the mean velocity has an almost ideal top-hat profile (as shown in figure 2*a*). The degree of turbulence, i.e. the ratio of the mean velocity to its root mean square, is smaller than one percent.

When normalized with respect to maximum velocity and width, the measured mean velocity profiles in the far field collapse into a single function, see figure 2(*b*). The profiles shown in figure 2 have not been shifted in the direction perpendicular to the mean flow, i.e. the maxima of all profiles are found at the centre of the jet. These features give evidence of the temporal stability of the jet.

As a further test of the experimental system, we measured the Taylor Reynolds number Re_λ (for the procedure of determination see below) as a function of the nozzle-based Reynolds number Re. The well-known square-root dependence as, for instance, reported by Naert (1995) of Re_λ on Re can be seen in figure 3. Note that we obtain a constant prefactor of 1.3 instead of 0.5 given by Naert (1995). It is likely that the different prefactors are due to the different inner profiles of the nozzles (R. A. Antonia, private communication).

3. Standard analysis

Next, we apply a standard analysis for turbulence to our data. The results are compared to typical results given in the literature. Our data set consists of 1.25×10^7 samples of the local velocity measured at a sampling frequency of 8 kHz. A lowpass filter (Stanford SR 640) at 20 kHz was used to suppress electronic noise. The sensor was placed in the centre of the jet at a distance of $125D$ from the nozzle. The velocity at the outlet of the nozzle was approximately $45.5\,\mathrm{m\,s^{-1}}$, which corresponds to a nozzle-based Reynolds number of about 2.7×10^4. The mean velocity in the centre of the jet at the distance of $125D$ had decreased to $2.25\,\mathrm{m\,s^{-1}}$ with a degree of turbulence of 17%. To obtain the spatial velocity dependence $u(x)$, we use Taylor's hypothesis of frozen turbulence. According to Taylor's hypothesis, the resolution in time corresponds to a spatial resolution of 0.28 mm.

For the integral length scale L, defined as

$$L = \int_0^{+\infty} R(r)\,\mathrm{d}r, \tag{3.1}$$

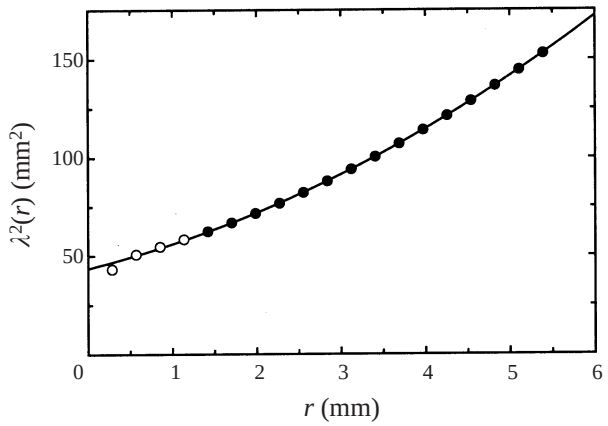

FIGURE 4. Estimation of the Taylor scale λ by extrapolation of $\lambda^2(r)$ (filled circles). The limit $r \to 0$ was performed by fitting a polynomial of degree two (solid line) to the data. Open circles denote the values used for the fit; values for r smaller than the spatial resolution of the sensor (1.25 mm) were neglected.

we find a value of 6.7 cm. $R(r)$ denotes the autocorrelation function of the velocity $u(x)$. Here and in the following, $u(x)$ denotes the fluctuating part of the local velocity, thus $\langle u(x) \rangle = 0$.

In order to calculate the Taylor scale λ, we used the method proposed by Aronson & Löfdahl (1993). For isotropic flows, λ^2 can be written as

$$\lambda^2 = \frac{\langle u(x)^2 \rangle}{\langle (\partial u/\partial x)^2 \rangle}. \tag{3.2}$$

The partial derivative is approximated by velocity increments. Thus, λ is obtained as

$$\lambda^2 = \lim_{r \to 0} \lambda^2(r),$$

$$\lambda^2(r) = \frac{\langle u(x)^2 \rangle r^2}{\langle v(r)^2 \rangle}. \tag{3.3}$$

The limit $r \to 0$ is performed by fitting a polynomial to $\lambda^2(r)$, which yields $\lambda = 6.6$ mm (see figure 4). The estimated λ enables us to determine the Taylor Reynolds number $Re_\lambda = 190$.

Another important scale for turbulence is the Kolmogorov length η, for which we obtain a value of 0.3 mm. Thus the active length of the sensor corresponds to a spatial resolution of 4η.

In order to validate the consistency of our data with well-known characteristics of turbulence, we performed a scaling analysis of the r-dependence of the moments and analysed the shape of the probability densities (p.d.f.(s)) $p(v, r)$ of the velocity increment $v(r)$.

Scaling can be seen in the power spectrum (figure 5). The scaling exponents ζ_n of the nth-moments of the increments as defined in equation (1.3) were evaluated using extended self-similarity (ESS) as proposed by Benzi *et al.* (1993). Figure 6 displays our results, which are in accordance with the values reported by Arneodo *et al.* (1996). We restrict our analysis to exponents of up to order eight. Figure 7 displays the function $v^8 p(v, r)$, which has to be integrated in order to obtain $\langle v(r)^8 \rangle$. It becomes evident that the wings of this function are not very well defined. The error of the

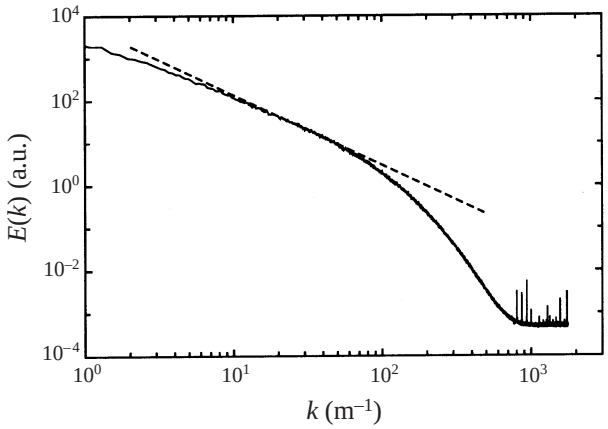

FIGURE 5. Power spectrum of the data set. The dashed line indicates scaling behaviour according to Kolmogorov (1941): $E(k) \propto k^{-5/3}$.

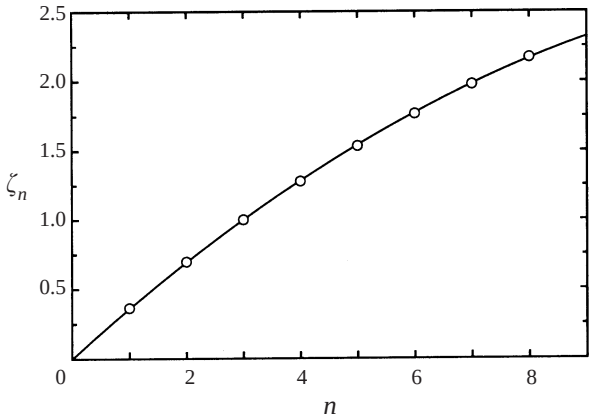

FIGURE 6. The scaling exponents ζ_n versus the order n, determined by ESS according to Benzi *et al.* (1993). Fitting the data according to Kolmogorov (1962) (solid line) yields $\mu = 0.227$ (see equation (1.6)). For the sixth-order exponent ζ_6 we obtain a value of 1.77 which is in agreement with the value of $\zeta_6 = 1.74 \pm 0.04$ given by Arneodo *et al.* (1996).

eighth-order moment is therefore already considerably high. As this problem increases with the order of the moment, the eighth-order moment is the highest one that can be determined from data with 10^7 samples with reasonable accuracy. (For a detailed quantitative discussion of this topic we refer the reader to the papers by Peinke *et al.* (1993, 1994).)

Another approach to characterize intermittency in turbulence is to evaluate the shape of the probability density functions $p(v, r)$ (see figure 8). We use the well-known formula given by Castaing *et al.* (1990) to parameterize the evolution of the shape of the p.d.f.(s) in r and to obtain the shape parameter Λ^2 as a function of r. As shown in figure 9, our results are in good agreement with previous ones obtained by Chabaud *et al.* (1994). We conclude that our data show the typical features of small-scale turbulence, i.e. the typical intermittency effects.

4. Theory of Markov processes

This section gives a brief summary of the theory of Markov processes, which will be of importance for our statistical analysis. (For further details of Markov processes

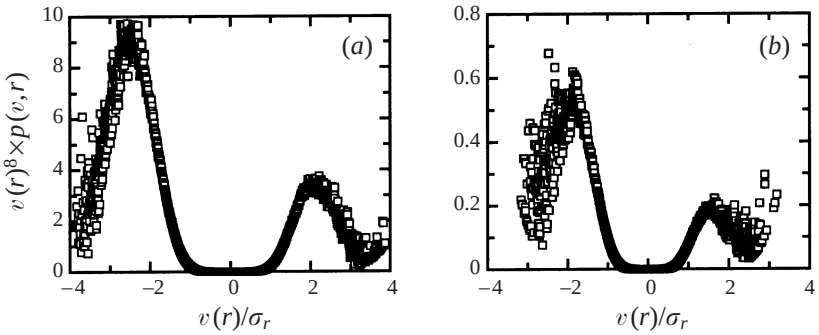

FIGURE 7. The product $v(r)^8 p(v,r)$ for the scales (*a*) $r = 1.0\,L$ and (*b*) $r = 0.2\,L$.

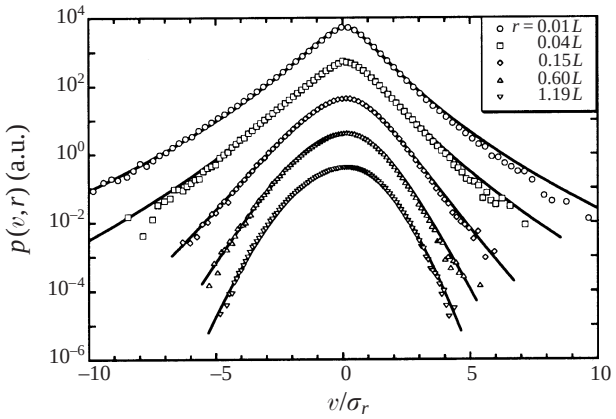

FIGURE 8. Probability density functions (p.d.f.(s)) of the velocity increment $v(r)$ at different scales r (symbols) and fits according to the formula given by Castaing *et al.* (1990) (lines). The p.d.f.(s) are normalized to their respective standard deviations σ_r and shifted in the vertical direction for clarity of presentation.

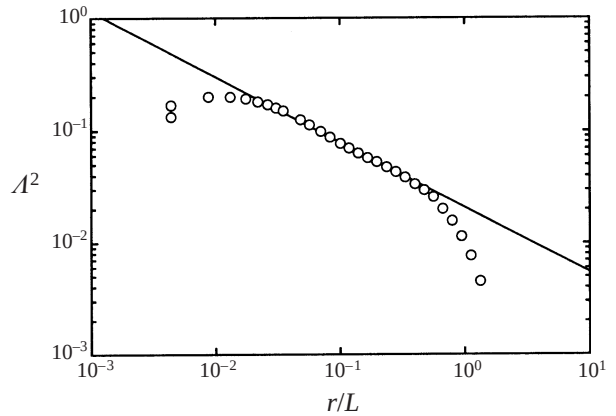

FIGURE 9. The shape parameter Λ^2 determined by fitting the p.d.f.(s) of the increment with Castaing *et al.*'s formula. Within the inertial range, Λ^2 can be described by a power law: $\Lambda^2 \propto r^{\beta}$. From the fit (straight line) we obtain $\beta = 0.59 \pm 0.01$ in agreement with the values given by Chabaud *et al.* (1994).

we refer the reader to the book by Risken (1984) and the paper by Hänggi & Thomas (1982).)

Fundamental quantities related to Markov processes are conditional probability density functions. Given the joint probability density $p(v_1, r_1; v_2, r_2)$ for finding the increments $v_1(:=v(r_1))$ at a scale r_1 and v_2 at a scale r_2 with $r_1 < r_2$, the conditional p.d.f. $p(v_1, r_1|v_2, r_2)$ is defined as

$$p(v_1, r_1|v_2, r_2) = \frac{p(v_1, r_1; v_2, r_2)}{p(v_2, r_2)}. \tag{4.1}$$

$p(v_1, r_1|v_2, r_2)$ denotes the conditional probability density for the increment v_1 at a scale r_1 given an increment v_2 at a scale r_2. It should be noted that the small scale r_1 lies within the larger scale r_2 (see equation (1.1): the increments v_1 and v_2 are calculated for the same reference point x).

Higher-order conditional probability densities can be defined in an analogous way:

$$p(v_1, r_1|v_2, r_2; \ldots; v_N, r_N) = \frac{p(v_1, r_1; v_2, r_2; \ldots; v_N, r_N)}{p(v_2, r_2; \ldots; v_N, r_N)}. \tag{4.2}$$

Again, the smaller scales r_i are nested inside the larger scales r_{i+1} (with the common reference point $\boldsymbol{x}$).

The stochastic process in r is a Markov process, if the conditional probability densities fulfil the following relations:

$$p(v_1, r_1|v_2, r_2; v_3, r_3; \ldots v_N, r_N) = p(v_1, r_1|v_2, r_2) \tag{4.3}$$

with $r_1 < r_2 < r_3 < \cdots < r_N$. As a consequence of (4.3), each N-point probability density $p(v_1, r_1; v_2, r_2; \ldots; v_N, r_N)$ can be determined as a product of conditional probability density functions:

$$p(v_1, r_1; \ldots v_N, r_N) = p(v_1, r_1|v_2, r_2) \ldots p(v_{N-1}, r_{N-1}|v_N, r_N) p(v_N, r_N). \tag{4.4}$$

Equation (4.4) indicates the importance of the conditional p.d.f. for Markov processes. Knowledge of $p(v, r|v_0, r_0)$ (for arbitrary scales r and r_0 with $r < r_0$) is sufficient to generate the entire statistics of the velocity increment encoded in the N-point probability density $p(v_1, r_1; v_2, r_2; v_3, r_3; \ldots; v_N, r_N)$.

For Markov processes the conditional probability density fulfils a master equation which can be put into the form of a Kramers–Moyal expansion:†

$$-r \frac{\partial}{\partial r} p(v, r|v_0, r_0) = \sum_{k=1}^{\infty} \left(-\frac{\partial}{\partial v} \right)^k D_k(v, r)\, p(v, r|v_0, r_0). \tag{4.5}$$

The Kramers–Moyal coefficients $D_k(v, r)$ are defined as the limit $\Delta r \to 0$ of the conditional moments $M_k(v, r, \Delta r)$:

$$D_k(v, r) = \lim_{\Delta r \to 0} M_k(v, r, \Delta r), \tag{4.6}$$

$$M_k(v, r, \Delta r) = \frac{r}{k!\Delta r} \int_{-\infty}^{+\infty} (\tilde{v} - v)^k\, p(\tilde{v}, r - \Delta r|v, r)\, \mathrm{d}\tilde{v}. \tag{4.7}$$

† Note that, in contrast to the usual definition as, for example, given by Risken (1984), we multiplied both sides of the Kramers–Moyal expansion by r (see also equation (4.7)). This is equivalent to the logarithmic length scale $\lambda = \ln(L/r)$ used by Friedrich & Peinke (1997). The negative sign of the left-hand side of equation (4.5) is due to the direction of the cascade toward smaller scales r.

For a general stochastic process, all Kramers–Moyal coefficients are different from zero. According to Pawula's theorem, however, the Kramers–Moyal expansion stops after the second term, provided that the fourth-order coefficient $D_4(v,r)$ vanishes. In that case, the Kramers–Moyal expansion reduces to a Fokker–Planck equation (also known as the backwards or second Kolmogorov equation):

$$-r\frac{\partial}{\partial r}p(v,r|v_0,r_0) = \left\{-\frac{\partial}{\partial v}D_1(v,r) + \frac{\partial^2}{\partial v^2}D_2(v,r)\right\} p(v,r|v_0,r_0). \tag{4.8}$$

D_1 is denoted the drift term, D_2 the diffusion term. The probability density $p(v,r)$ has to obey the same equation:

$$-r\frac{\partial}{\partial r}p(v,r) = \left\{-\frac{\partial}{\partial v}D_1(v,r) + \frac{\partial^2}{\partial v^2}D_2(v,r)\right\} p(v,r). \tag{4.9}$$

We remind the reader that the Fokker–Planck equation describes the probability density function of a stochastic process generated by the Langevin equation (we use Ito's definition)

$$-r\frac{\partial}{\partial r}v(r) = D_1(v,r) + \sqrt{D_2(v,r)}f(r) \tag{4.10}$$

where $f(r)$ is a δ-correlated Gaussian white noise.

Here, the increment $v(r)$ at a fixed point x is generated by a stochastic process with respect to the continuous variable r. Thus, we consider snapshots of velocity increments of the turbulent field as a function of r.

From the Kramers–Moyal expansion (4.5), which is also valid for the probability density $p(v,r)$, differential equations for the nth-order structure function are derived. By multiplication with v^n and integration with respect to v we obtain

$$\begin{aligned} -r\frac{\partial}{\partial r}\langle v^n(r)\rangle &= \sum_{k=1}^{\infty}(-1)^k \int_{-\infty}^{+\infty} v^n \left(\frac{\partial}{\partial v}\right)^k D_k(v,r)\, p(v,r)\, \mathrm{d}v \\ &= \sum_{k=1}^{n} \frac{n!}{(n-k)!}\int_{-\infty}^{+\infty} v^{n-k} D_k(v,r)\, p(v,r)\, \mathrm{d}v. \end{aligned} \tag{4.11}$$

Let us now consider a constructed simple case:

$$D_k(v,r) = d_k v^k, \tag{4.12}$$

with constant d_k. Then, we obtain

$$-r\frac{\partial}{\partial r}\langle v^n(r)\rangle = \sum_{k=1}^{n}\frac{n!}{(n-k)!}d_k\langle v^n(r)\rangle. \tag{4.13}$$

This equation implies scaling behaviour as discussed in § 1, equation (1.3). The exponents are

$$\zeta_n = -\sum_{k=1}^{n}\frac{n!}{(n-k)!}d_k. \tag{4.14}$$

Thus, we obtain a representation of the scaling indices in terms of the prefactors d_k of the Kramers–Moyal coefficients. If only d_1 and d_2 are different from zero we obtain

$$\zeta_n = -d_1 n - n(n-1)d_2. \tag{4.15}$$

In relating this behaviour to the statistics of velocity increments (with the condition

$\zeta_3 = 1$), we arrive at Kolmogorov's log-normal model, see equation (1.6). The corresponding stochastic process is the following simple one:

$$-r\frac{\partial}{\partial r}v(r) = -d_1 v(r) + \sqrt{d_2}v(r)f(r). \tag{4.16}$$

Note that this corresponds to a pure multiplicative stochastic process.

5. Experimental results

The hypothesis concerning the Markovian properties of turbulent data sets immediately fixes a framework for the analysis of the experimental data. First, one has to give evidence of the Markovian properties according to equation (4.3). Secondly, the evolution of conditional probability densities $p(v, r|v_0, r_0)$ has to be specified on the basis of the stochastic evolution equation, (4.5). To this end, we have to determine the conditional moments $M_k(v, r, \Delta r)$ at different scales r for various values of Δr.

Practically, it is only possible to evaluate the lowest-order coefficients. Therefore, we shall restrict our analysis to the coefficients of order one, two, and four. Approximating the limit $\Delta r \to 0$, we obtain the Kramers–Moyal coefficients $D_k(v, r)$. If the fourth-order coefficient vanishes, the evolution equation (4.5) takes the form of a Fokker–Planck equation, according to Pawula's theorem. Since we consider experimental data, we can only give upper bounds for the influence of higher-order terms, and we are not able to conclude rigorously that the spatial evolution of the conditional probability density obeys a Fokker–Planck equation. To verify our results, we compare the numerical solutions of the Fokker–Planck equations (4.8) and (4.9) with the probability density functions determined directly from the measured data.

For the rest of the article, velocities and velocity increments are given in units of σ_∞, which is defined according to

$$\sigma_\infty^2 = \lim_{r\to\infty}\langle v(r)^2\rangle. \tag{5.1}$$

For our data set, σ_∞ is $0.54\,\mathrm{m\,s^{-1}}$.

5.1. *Markovian properties*

Here we give evidence that the Markovian property (4.3) holds. Strictly speaking, the relationships (4.3) have to be verified for all positive values of N as well as for each set of scales $r_1, \ldots, r_N$, a task which is clearly impossible. Nevertheless, experimental data with typically 10^7 samples allow condition (4.3) to be verified for $N = 3$:

$$p(v_1, r_1|v_2, r_2; v_3, r_3) = p(v_1, r_1|v_2, r_2). \tag{5.2}$$

In figure 10, the contour plots of $p(v_1, \lambda|v_2, L/2)$ and $p(v_1, \lambda|v_2, L/2; v_3 = 0, L)$ have been superposed (λ denotes the Taylor microscale, L the integral scale). The proximity of corresponding contour lines yields evidence for the validity of equation (5.2) for the chosen set of length scales. Additionally, two cuts through the conditional probability densities are provided for fixed values of v_2.

Figure 11 shows the same plots for a different set of length scales: $r_1 = L/2 - \lambda/4$, $r_2 = L/2$ and $r_3 = L/2 + \lambda/4$. In this case, the contour lines clearly deviate from each other: the necessary condition for a Markov process is violated.

So far, our results suggest that the condition (5.2) holds for large-scale differences $r_{i+1} - r_i$, whereas it is violated for smaller differences. In order to investigate the

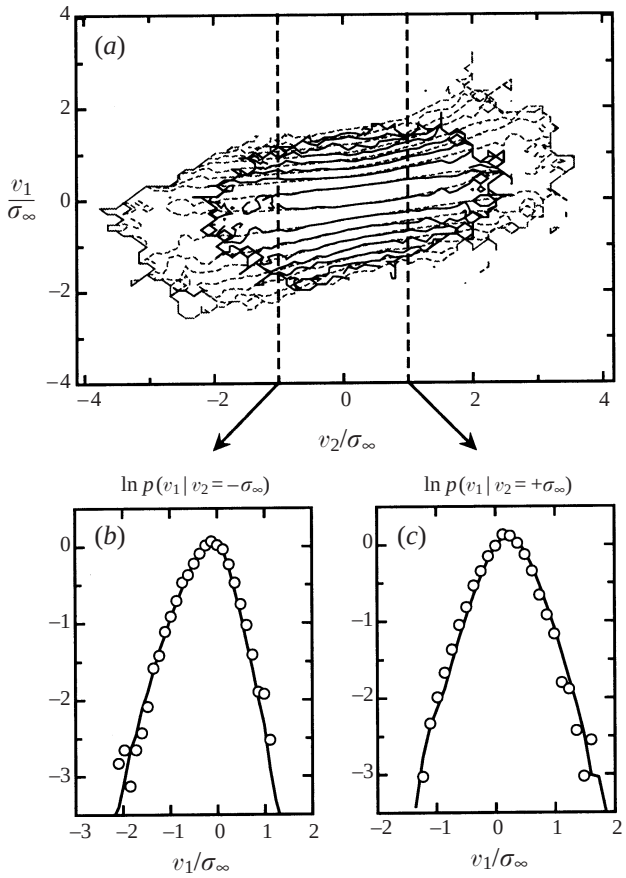

FIGURE 10. (*a*) Contour plots of the conditional p.d.f.(s) $p(v_1, r_1|v_2, r_2)$ (dashed lines) and $p(v_1, r_1|v_2, r_2; v_3 = 0, r_3)$ (solid lines) for $r_1 = \lambda$, $r_2 = L/2$ and $r_3 = L$. (*b*, *c*) Cuts through the conditional p.d.f.(s) for $v_2 = +\sigma_\infty$ and $v_2 = -\sigma_\infty$. Symbols: $p(v_1, r_1|v_2, r_2; v_3 = 0, r_3)$, lines: $p(v_1, r_1|v_2, r_2)$.

crossover range between these two scales, we have performed a statistical test, the so-called Wilcoxon test (a detailed description of the test is given in Appendix A).

For a chosen set of length scales r_1, r_2 and r_3, we calculate the normalized expectation value $\langle t \rangle$ of the number of inversions of the conditional velocity increments $v_1|_{v_2}$ and $v_1|_{v_2,v_3}$. If condition (5.2) holds, $\langle t \rangle$ has a value of $\sqrt{2/\pi} \approx 0.8$. Values of $\langle t \rangle$ larger than this indicate that equation (5.2) is violated.

The expectation value $\langle t \rangle$ is a function of the velocity increment v_3 and the length scales r_1, r_2, and r_3. In order to reduce the number of parameters, we chose v_3 to be zero and the differences $r_3 - r_2$ and $r_2 - r_1$ to be equal: $\Delta r = r_3 - r_2 = r_2 - r_1$.

In figure 12, $\langle t \rangle$ is plotted as a function of Δr for several scales r_1. While we obtain a value close to $\sqrt{2/\pi}$ for large Δr, the Markov condition is violated for small values of the separation Δr. The scale at which this crossover takes place is close to the Taylor scale λ and does not sensitively depend on the choice of r_1. We should note that these results are consistent with previous findings obtained by Friedrich, Zeller & Peinke (1998*b*) with different stochastic measures.

The cascade can therefore be regarded as a Markov process on length scales larger than the finite step of length λ. In units of this step size, the noise f acting on

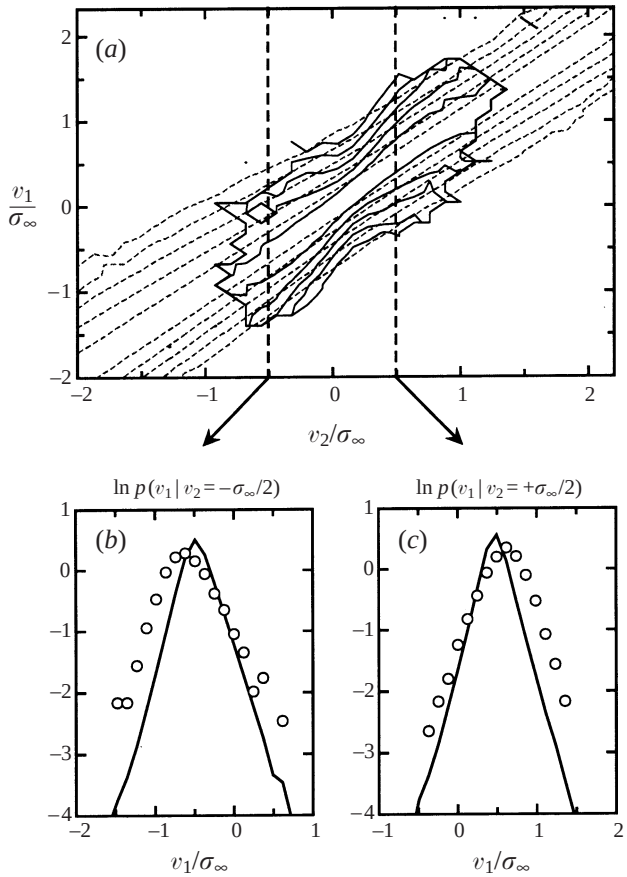

FIGURE 11. As figure 10 but for $r_1 = L/2$, $r_2 = L/2 + \lambda/4$ and $r_3 = L/2 + \lambda/2$.

the stochastic process (see equation (4.10)) can be taken to be δ-correlated. Such finite step sizes are a common feature of physical stochastic processes. In the case of Brownian motion, the mean free path of the molecules defines a similar finite length. The process can be considered to be Markovian on scales larger than this elementary length scale. For turbulent flows, this elementary step seems to be of the order of the Taylor length scale. Preliminary results on data with different Reynolds numbers indicate that the Markov length is always close to the Taylor microscale, independent of the Reynolds number (we examined data sets with $100 \leqslant Re_\lambda \leqslant 1000$) and the experimental setup (we analysed data from free jet experiments, grid turbulence, and the wake flow of a cylinder).

5.2. *Kramers–Moyal coefficients*

According to equations (4.1) and (4.7), the coefficients $M_k(v, r, \Delta r)$ can be calculated from the joint probability density functions. These joint p.d.f.(s) $p(\tilde{v}, r - \Delta r; v, r)$ are easily obtained from the experimental data by counting the number $N(\tilde{v}, v)$ of occurrences of the two increments $\tilde{v}$ and v. Assuming the error of $N(\tilde{v}, v)$ to be given by $\sqrt{N(\tilde{v}, v)}$, errors for the coefficients $M_k(v, r, \Delta r)$ can be derived.

Figure 13 shows the results for M_1 and M_2 at the scale $r_1 = L/2$ for $\Delta r = \lambda$. The coefficient M_1 shows a linear dependence on the velocity increment with small second- and third-order-term corrections, while M_2 can be approximated by a polynomial of

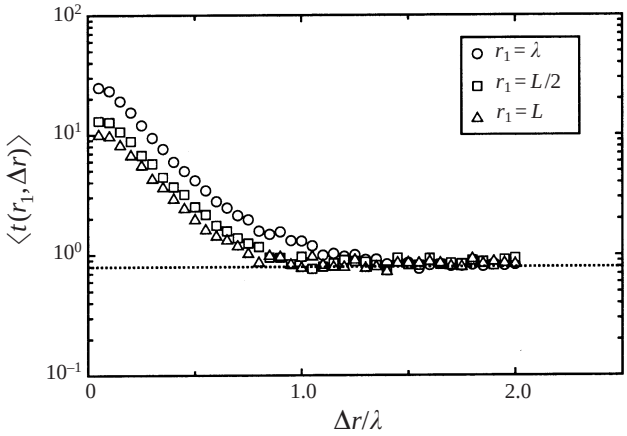

FIGURE 12. The expectation value $\langle t(r_1, \Delta r)\rangle$ as defined in Appendix A plotted as a function of Δr for several values of r_1.

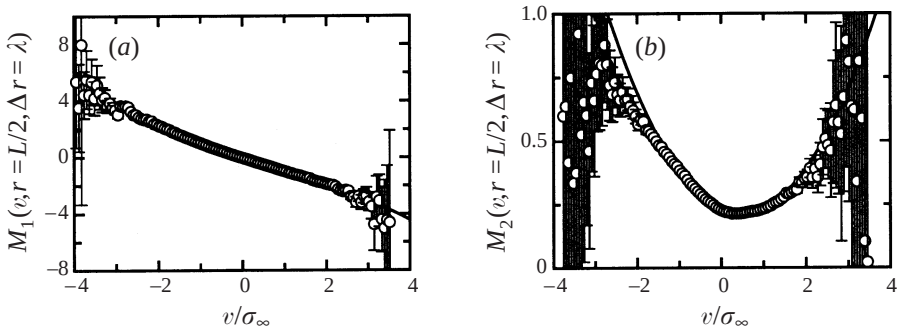

FIGURE 13. The coefficients (*a*) $M_1(v, r, \Delta r)$ and (*b*) $M_2(v, r, \Delta r)$ as a function of the velocity increment v for $r = L/2$ and $\Delta r = \lambda$ (symbols). M_1 is fitted by a ploynomial of degree three, M_2 by a polynomial of degree two (lines).

degree two in v:

$$\left.\begin{aligned} M_1(v, r, \Delta r) &= O(r, \Delta r) - G(r, \Delta r)v + K(r, \Delta r)v^2 - E(r, \Delta r)v^3, \\ M_2(v, r, \Delta r) &= A(r, \Delta r) - D(r, \Delta r)v + B(r, \Delta r)v^2. \end{aligned}\right\} \tag{5.3}$$

This behaviour occurs for all scales r and all values of Δr. Therefore, it is reasonable to assume that the same v-dependence holds also for the Kramers–Moyal-coefficients:

$$\left.\begin{aligned} D_1(v, r) &= o(r) - \gamma(r)v + \kappa(r)v^2 - \epsilon(r)v^3, \\ D_2(v, r) &= \alpha(r) - \delta(r)v + \beta(r)v^2, \end{aligned}\right\} \tag{5.4}$$

and that the limit $\Delta r \to 0$ in equation (4.6) can be performed:

$$o(r) = \lim_{\Delta r \to 0} O(r, \Delta r), \quad \gamma(r) = \lim_{\Delta r \to 0} G(r, \Delta r), \quad \text{etc.} \tag{5.5}$$

Figure 14 shows the slope $G(r, \Delta r)$ of M_1 for several values of Δr at scale $r = L/2$. For values of $\Delta r > \lambda$, where the Markov condition is fulfilled, G exhibits a linear dependence on Δr, whereas in the range $\Delta r < \lambda$, G deviates significantly from that linear behaviour. Extrapolating G towards $\Delta r = 0$ using a linear fit in the interval $\lambda \leqslant \Delta r \leqslant 2\lambda$, we obtain the slope γ of $D_1(v, r)$ for $r = L/2$.

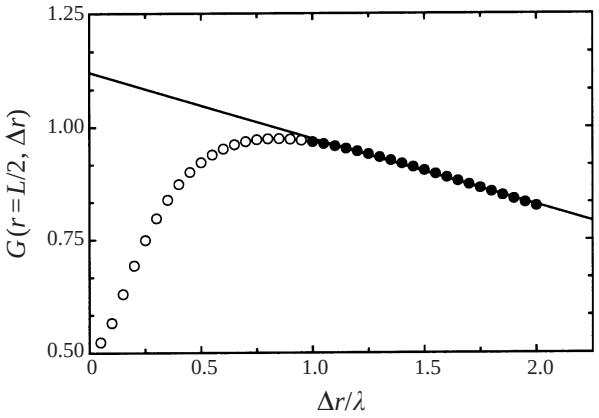

FIGURE 14. The slope $G(r, \Delta r)$ of the coefficient $M_1(v, r, \Delta r)$ as a function of Δr for $r = L/2$ (filled circles). For $\Delta r > \lambda$, a linear dependence in Δr is observed. The limit $\Delta r \to 0$ is performed by fitting a line to the data with $r > \lambda$. Values for $r < \lambda$ (open circles) have been rejected as they lie within the range of scales for which the Markov properties are not fulfilled.

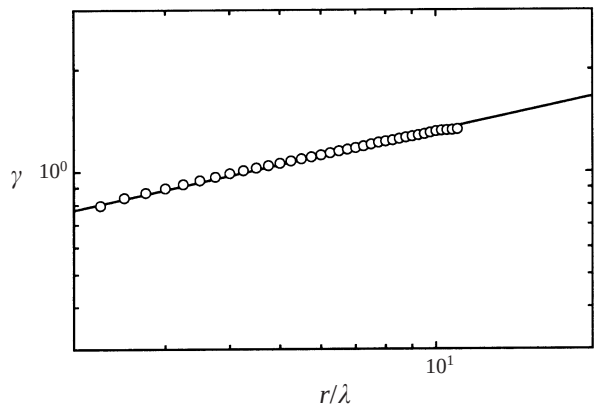

FIGURE 15. The slope $\gamma(r)$ of $D_1(v, r)$ as a function of r (circles). Throughout the inertial range, γ is fitted well by $\gamma(r) = \gamma_0(r/\lambda,)^{1/3}$ (straight line). The fit yields $\gamma_0 = 0.61$.

Performing this procedure at several scales r, we are able to determine the slope γ as a function of r. As shown in figure 15, γ turns out to be proportional to $r^{1/3}$ throughout the inertial range $\lambda \leqslant r \leqslant L$.

Let us summarize our results for the coefficients D_1 and D_2 ($\rho := r/\lambda$):

$$\left.\begin{aligned} &D_1(v,r) = -o(r) - \gamma(r)v + \kappa(r)v^2 - \epsilon(r)v^3, \\ &\quad o(r) = 0.0015\rho^{1.6}, \quad \gamma(r) = 0.61\rho^{1/3}, \quad \kappa(r) = 0.0096\rho, \quad \epsilon(r) = 0.0023\rho^{1.3}; \\ &D_2(v,r) = \alpha(r) - \delta(r)v + \beta(r)v^2, \\ &\quad \alpha(r) = 0.033\rho^{1.25}, \quad \delta(r) = 0.011\rho^{1.2}, \quad \beta(r) = 0.061\rho^{0.23}. \end{aligned}\right\} \tag{5.6}$$

We should note that the functional dependences of the coefficients $o(r)$, $\gamma(r), \ldots$ on r given above are merely parametrizations of our experimental results. Power laws were chosen, because they turned out to describe the measured values with sufficient

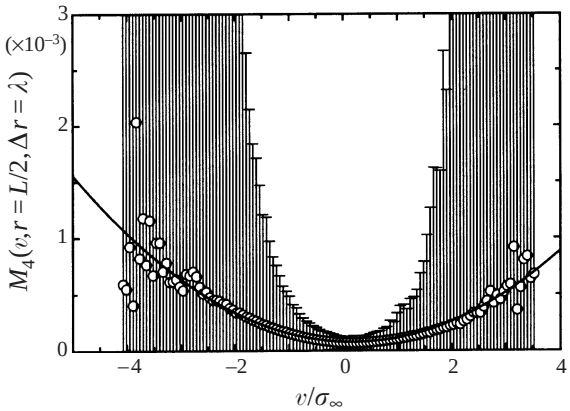

FIGURE 16. The coefficient $M_4(v, r, \Delta r)$ as a function of the velocity increment v for $r = L/2$ and $\Delta r = \lambda$ (circles) and the fitting polynomial of degree two (line).

accuracy. However, further theoretical investigations may lead to slightly different functional dependences.†

5.3. *The fourth-order coefficient*

Pawula's theorem shows that it is of importance to estimate the fourth-order coefficient and to decide whether it may be neglected. Figure 16 shows the experimental result for $M_4(v, r = L/2, \Delta r = \lambda)$. M_4 is finite, although it is significantly smaller than the second-order coefficient M_2. A remarkable result is that the errors of $M_4(v, r, \Delta r)$ for small $|v|$ are in the order of magnitude of the values themselves, and that for increasing $|v|$ they become much larger than the values. This is a first hint that within the experimental limitations it is not possible to decide whether D_4 is finite or zero.

The dependence of $M_4(v, r, \Delta r)$ on the velocity increment turns out to be fitted well by a polynomial of order two in v with coefficients C_i depending on r and on Δr (see figure 16). Again, we assume that $D_4(v, r)$ shows the same dependence on v and that the coefficients $c_i(r)$ can be obtained from the $C_i(r, \Delta r)$:

$$\left.\begin{aligned} D_4(v, r) &= c_0(r) - c_1(r)v + c_2(r)v^2, \\ c_i(r) &= \lim_{\Delta r \to 0} C_i(r, \Delta r). \end{aligned}\right\} \tag{5.7}$$

Performing the limit $\Delta r \to 0$ according to equation (5.7), we obtain ($\rho = r/\lambda$):

$$c_0(r) = 4.31 \times 10^{-6}\rho^{1.15}, \quad c_1(r) = 1.15 \times 10^{-5}\rho^{1.21}, \quad c_2(r) = 9.20 \times 10^{-5}\rho^{-0.33}. \tag{5.8}$$

These values are smaller by at least a factor of 10^{-3} than the corresponding values for D_2. But the question of whether they are small enough to be neglected still remains open. A quantitative measure for the influence of D_4 can be obtained from the equation for the velocity structure functions (4.11). This equation shows that the influence of higher-order Kramers–Moyal coefficients on $\langle v(r)^n \rangle$ increases with order n. Therefore, to prove that D_4 can be neglected, it is sufficient to prove that it has

† It may be worth pointing out that the results given on D_1 and D_2 may be interpreted as a result of a projection of the high-dimensional problem of turbulence on the subspace of longitudinal velocity increments. A more sophisticated, multidimensional analysis (including, for example, tranversal increments or the energy dissipation rate) will probably lead to simpler Kramers–Moyal coefficients, which might be interpreted more easily. Similar improvements are expected for higher Reynolds numbers.

no influence on the highest-order moment that can be measured. Furthermore, it is easily seen from this and the subsequent argumentation that, provided we can neglect D_4, all higher orders D_k can be neglected, too.

As shown previously (see figure 7), the eighth-order structure function is the highest-order moment that can be determined accurately from a data set with only 10^7 samples. Equation (4.11) for $n = 8$ reads

$$\begin{aligned} -r\frac{\partial}{\partial r}\langle v(r)^8\rangle = 8 &\int_{-\infty}^{+\infty} v^7 D_1(v,r)\, p(v,r)\,\mathrm{d}v \\ &+ \underbrace{8\times 7\int_{-\infty}^{+\infty} v^6 D_2(v,r)\, p(v,r)\,\mathrm{d}v}_{T_2(r)} \\ &+ 8\times 7\times 6\int_{-\infty}^{+\infty} v^5 D_3(v,r)\, p(v,r)\,\mathrm{d}v \\ &+ \underbrace{8\times 7\times 6\times 5\int_{-\infty}^{+\infty} v^4 D_4(v,r)\, p(v,r)\,\mathrm{d}v}_{T_4(r)} \\ &+ \cdots . \end{aligned} \tag{5.9}$$

In order to estimate the influence of D_4 in equation (5.9), we compare the term $T_4(r)$ with $T_2(r)$. In particular, we will look for an upper bound of the ratio T_4/T_2. A simple estimation (see Appendix B) allows us to express this ratio in terms of the coefficients $c_i(r)$ and the constant term $\alpha(r)$ of D_2:

$$\frac{T_4(r)}{T_2(r)} \leqslant \frac{6\times 5(c_0(r)+c_1(r)+c_2(r))}{\alpha(r)} = X(r). \tag{5.10}$$

The measured values of $X(r)$ are smaller than 10% throughout the inertial range, see figure 17. In addition, the calculation shows that the relation $\leqslant$ in (5.10) might well be replaced by $\ll$ (see Appendix B). We therefore conclude that D_4 does not have an important influence on the evolution of the eighth-order structure function. Based on this result, we will proceed with the assumption that Pawula's theorem applies, i.e. we assume that the Markov process is described by a Fokker–Planck equation. The physical meaning of this result is that the noise $f(r)$ acting on the process (see equation (4.10)) can be taken to be Gaussian distributed in addition to its δ-correlation (see § 5.1).

5.4. *Solutions of the Fokker–Planck equation*

The results and assumptions of the preceding sections lead to Fokker–Planck equations for the p.d.f. $p(v,r)$ and the conditional p.d.f. $p(v,r|v_0,r_0)$, respectively (equations (4.9) and (4.8)). The functions $D_1(v,r)$ and $D_2(v,r)$ can be estimated from experimental data. The result for $D_1(v,r)$ shows a linear behaviour in v with small second- and third-order-term corrections, while $D_2(v,r)$ was found to be quadratic in v (see (5.6)).

In order to test these results, we compared the (numerical) solutions of the Fokker–Planck equation with the probability density functions obtained directly from the data. It turned out that the agreement of the numerical solution with the experimental data improves if some of the numerical values for D_2 in (5.6) are slightly modified. The best result was found by decreasing the values of the prefactors of $\delta(r)$ and $\beta(r)$, the linear and quadratic term in D_2, respectively, from 0.011 to 0.009 for δ and from 0.061 to 0.043 for β.

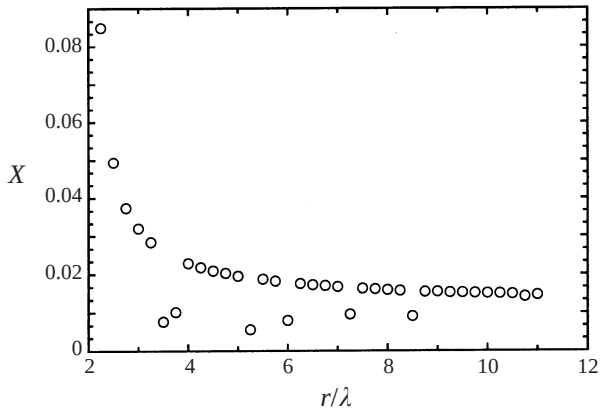

FIGURE 17. The ratio X, defined in § 5.3, as a function of scale r.

The reason for the discrepancy between these values and the ones given in (5.6) can be traced back to the method used to fit the coefficient $M_2(v, r, \Delta r)$. From figure 13 it becomes evident that the fit, which weighs data points by the inverse of their error, overestimates the wings of M_2. Furthermore, the deviations of the fit from the data are higher for negative values of v than for positive ones. Therefore, it turns out that, in order to describe the wings of D_2 as well as the minimum in the vicinity of $v = 0$, the coefficients δ and β have to be chosen smaller than suggested by the fit.

Figure 18, which compares the solutions of the Fokker–Planck equation with the experimental data for the p.d.f. $p(v, r)$, proves that a Fokker–Planck equation accurately describes the evolution of $p(v, r)$ in r.

As mentioned above, the Fokker–Planck equation also governs the conditional p.d.f. $p(v, r|v_0, r_0)$. As a further test of our results, we calculated the solutions of the Fokker–Planck equation (4.8). Figure 19 shows the result, again in comparison with measured data, for $p(v, r = 0.6L|v_0, r_0 = L)$. Taking into account the various uncertainties in the determination of the coefficients D_1 and especially D_2, the agreement between the solution of (4.8) and the data is remarkably good.

6. Discussion

The purpose of the present article was to show how the mathematical framework of Markov processes can be applied to develop a successful statistical description of fully developed, homogeneous, and isotropic turbulence. Within the experimental limitations we were able to verify the Markovian properties of the statistics of the velocity increment for scales (and differences of scales) larger than the Taylor scale. Additionally, we evaluated the evolution equation for the conditional probability densities, the so-called Kramers–Moyal expansion.

Furthermore, it is shown that this expansion can be approximated by a Fokker–Planck equation, i.e. the terms of order three and higher are negligible. The comparison of the solutions of the resulting Fokker–Planck equation with the experimental data strongly supports our results for the coefficients D_1 and D_2.

Summarizing, we would like to point out that the theory of Markov processes enables us to *measure* the differential equation describing the evolution of the p.d.f.(s) of the velocity increment without using any additional models or assumptions. In other words, we showed that, by analysing experimental data, it is possible to extract

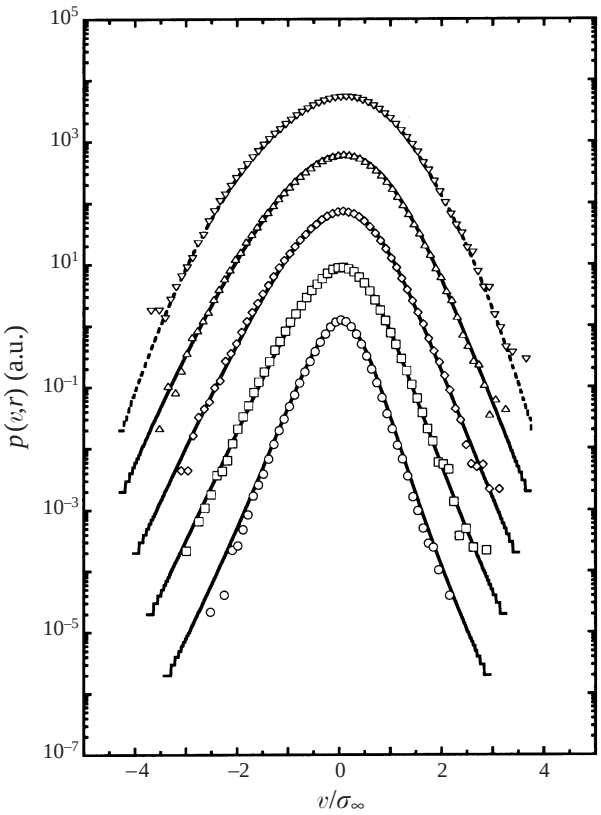

FIGURE 18. Comparison of the numerical solution of the Fokker–Planck equation (solid lines) for the p.d.f.(s) $p(v,r)$ with the p.d.f.(s) obtained directly from the experimental data (symbols). The scales r are (from top to bottom): $r = L, 0.6L, 0.35L, 0.2L$ and $0.1L$. The p.d.f. at the largest scale L was parametrized (dashed line) and used as initial condition for the Fokker–Planck equation. The p.d.f.(s) have been shifted in the vertical direction for clarity of presentation.

a stochastic equation for the turbulent cascade describing the small-scale structure of turbulence.

The results presented above have some impact on theoretical as well as on experimental considerations.

First we would like to comment on the connection between our results and the scaling behaviour of the structure functions. It can easily be shown that the equation for the r-evolution of the structure functions, equation (C 5) (Appendix C), is solved by a simple scaling ansatz ($S_v^n(r) \propto r^{\zeta_n}$) for the case where α and δ are zero and γ as well as β are constant in r (see also equation (4.15)). The facts that neither α nor δ are zero and that γ strongly depends on r are in contrast to such a simple assumption. The connection to scaling is therefore more complicated. Indeed, the r-dependence of the coefficients γ, α, ... is not necessarily in contradiction to a (at least approximate) scaling behaviour of the structure functions. Assuming strict scaling behaviour for e.g. the third-order structure function, equation (C 5) merely imposes a certain condition on the relation between the coefficients $\gamma(r)$, $\beta(r)$, $\delta(r)$ and the second-order structure function. However, quantitative investigations concerning this issue would be performed better on data sets at very high Reynolds number which

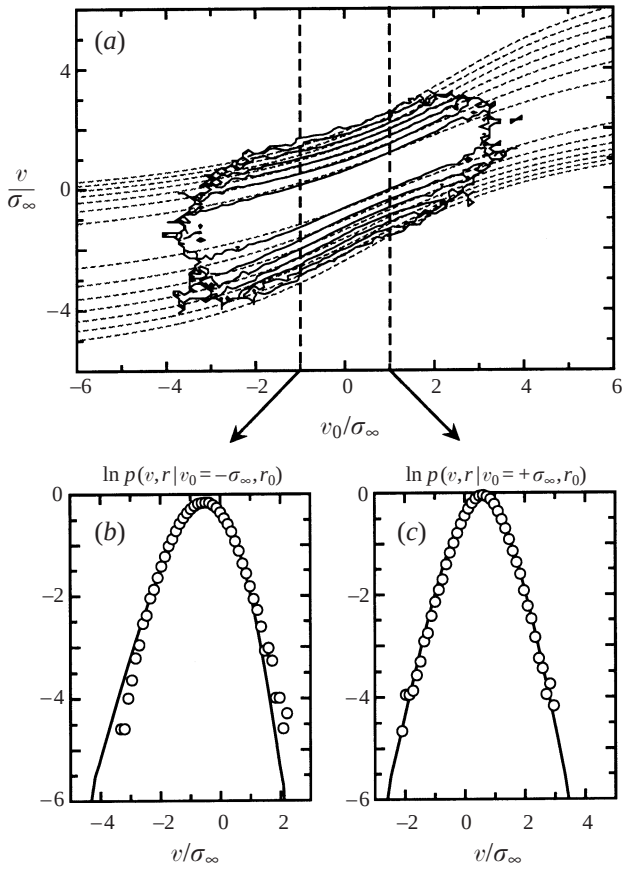

FIGURE 19. Comparison of the numerical solution of the Fokker–Planck equation for the conditional p.d.f. $p(v,r|v_0,r_0)$ with the experimental data. (*a*) Contour plots of $p(v,r|v_0,r_0)$ for $r_0 = L$ and $r = 0.6L$. Dashed lines: numerical solution of (4.8), solid lines: experimental data. (*b*, *c*) Cuts through $p(v,r|v_0,r_0)$ for $v_0 = +\sigma_\infty$ and $v_0 = -\sigma_\infty$ respectively. Symbols: experimental data, lines: numerical solution of the Fokker–Planck equation.

exhibit an extended scaling regime for the third-order moment and for which D_1 is given by the simple form (C 1).

We would also like to comment on the use of the absolute value of the velocity increment, which is widely used to analyse velocity structure functions, cf. Benzi *et al.* (1993), Arneodo *et al.* (1996). From the Fokker–Planck equation for the probability density function $p(v,r)$, it is possible not only to derive equations for the structure functions $S_v^n(r)$, but also for the moments T_v^n of the absolute value of the velocity increment (see Appendix C). The equations for odd-order moments exhibit fundamental differences between $S_v^n(r)$ and $T_v^n(r)$ due to the non-vanishing values of the coefficients $\alpha(r)$ and $\delta(r)$, the constant and linear term in D_2, respectively. As shown in Appendix C, those differences are by no means negligible. Thus one has to be more cautious when replacing $S_v^n(r)$ by $T_v^n(r)$ as is commonly done, especially in the case of low Reynolds number data.

The differences between $T_v^n(r)$ and $S_v^n(r)$ for uneven values of n are caused by the constant and linear terms of D_2, $\alpha(r)$ and $\delta(r)$. Furthermore, it has recently been shown by Amblard & Brossier (1999) that the existence of those terms is in contradiction to

the propagator approach by Castaing *et al.* Therefore, the question arises of whether our results for α and δ are significant. As pointed out by Amblard & Brossier (1999), those coefficients stem from a second-order quantity, namely the diffusion coefficient D_2, which is much more affected by experimental noise than the first-order coefficient D_1. (The growing influence of noise on the Kramers–Moyal coefficients can be seen by comparing figures 13 and 16.) On the other hand, it becomes evident from figure 13(*b*) that noise mainly acts on the wings of D_2, while in the vicinity of $v = 0$ the function $D_2(v, r)$ is well defined. Therefore, the coefficient of the fitting polynomial that can be determined best (i.e. which has the smallest relative error) is the zero-order coefficient α. Hence, the experiment definitely yields non-zero values for the coefficients α and δ. (However, the above-mentioned preliminary results on a data set with $Re_\lambda = 1000$ indicate that α and δ are decreasing functions of the Reynolds number, while β seems to increase slightly with Re.)

Our findings are consistent with the well-documented fact that the maxima of the p.d.f.(s) $p(v, r)$ are Gaussian. It is known that a Fokker–Planck equation with a diffusion coefficient constant in v (i.e. $D_2 = \alpha(r)$) has Gaussian solutions. As D_2 can be approximated by α for small values of $|v|$, the p.d.f.s are close to Gaussians near $v = 0$. It is also well-known that the maxima of $p(v, r)$ become steeper for higher Reynolds numbers, which should result in a decrease of the coefficient α. Comparing our analysis presented here with an analogous analysis of other data (e.g. inhomogeneous turbulence (Lück *et al.* 1999), financial data (Ghashghaie *et al.* 1996; Friedrich *et al.* 2000*a*), and surface roughness (Friedrich *et al.* 1998*a*)) we see that the sharpness of the maximum of the p.d.f.(s) is closely related to the size of α. Only for very sharp p.d.f.(s) does α become close to zero.

Next, our result is discussed for the Langevin equation (4.10). Based on (C 1) the Langevin equation can be taken to be of the form

$$-r\frac{\partial}{\partial r}v(r) = -\gamma(r)v(r) + \sqrt{\alpha}f_1(r) + \sqrt{\beta}v(r)f_2(r). \tag{6.1}$$

Here, we have introduced two noise sources $f_1(r)$ and $f_2(r)$. In order to obtain a diffusion term $D_2(v, r)$ depending linearly on v we have to assume that the two fluctuating forces $f_1(r)$ and $f_2(r)$ are correlated, where the cross-correlation is proportional to the linear coefficient of D_2, δ:

$$\langle f_1(r)f_2(r)\rangle \approx \delta(r - r')\delta. \tag{6.2}$$

As pointed out by Dubrulle (2000), this correlation has an important physical impact: assuming an even probability density at large scales (corresponding to vanishing flux $\langle v(r)^3\rangle$), the stochastic process across scales generates skewness of the probability densities due to correlation of additive and multiplicative noise sources.

The finding of a finite step size in the Markov process can be related to recently proposed features of small-scale turbulence. We have presented evidence that below a certain value of Δr the Markov properties are not valid any more. This means that a description of the disorder cannot be achieved by a one-dimensional Langevin equation for such small scales. Either more variables or higher-order derivatives with respect to r in the Langevin equation have to be taken into account. This indicates some structural change of the disordered field, as may be caused by small-scale coherent structures. Recently, Hatakeyama & Kambe (1997) have shown that the statistics of turbulence can be modelled well by a random arrangement of small-scale Burger vortices (typical size in the range of the Taylor microlength), see also Jimenez & Wray (1998). The presence of this finite step size throughout the whole cascade

might also cause problems in the determination of fusion rules as discussed by L'vov & Procaccia (1996) and Fairhall *et al.* (1997).

This indicates the importance of increasing the understanding of the viscous subrange of turbulence. For our experimental data it is difficult to extract more features, because the viscous length scale is close to the finite resolution of our sensors.

Summarizing, we have provided attempts to characterize N-point density functions $p(v_1, r_1; \ldots; v_N, r_N)$ of velocity increments of turbulent fields. This characterization is facilitated by the observation of Markovian properties which allows the N-point distribution $p(v_1, r_1; \ldots; v_N, r_N)$ to be generated by a product of conditional probability densities $p(v_i, r_i | v_{i+1}, r_{i+1})$. In the limit $\Delta r \to 0$ a path integral representation of the probability density function is obtained, see Risken (1984). This limit has to be taken in the sense of $Re \to \infty$, where the Taylor length and the step size of the cascade become zero. In our opinion, this path integral representation is a suitable representation of the probability density of systems with flux equilibrium and plays a similar role as the Gibbs distribution for equilibrium systems.

We acknowledge helpful discussions with F. Chilla, M. Greiner, P. Haenggi, T. Kambe, St. Lück, A. Naert, J.-F. Pinton and B. Reisner. This work was partially supported by the DFG-grant Pe 478/3.

Appendix A. The Wilcoxon test

Consider two stochastic variables x and y. In the present case, x denotes the velocity increment v_1 on scale r_1, where the increment v_2 has been observed at scale r_2; y is the increment v_1 on a scale r_1 under the condition that the increments v_2 and v_3 are given at scales r_2 and r_3, respectively:

$$\left.\begin{aligned} x(v_2, r_1, r_2) &= v_1(r_1)|_{v_2(r_2)}, \\ y(v_2, v_3, r_1, r_2, r_3) &= v_1(r_1)|_{v_2(r_2), v_3(r_3)}. \end{aligned}\right\} \tag{A 1}$$

The hypothesis to be tested is

$$p(x) = \tilde{p}(y), \tag{A 2}$$

where the probability density functions p and $\tilde{p}$ both are unknown.

Two samples $x_1, \ldots, x_n$ and $y_1, \ldots, y_m$ of independent realizations of x and y, respectively, are taken from the data and sorted in ascending order. One obtains a series like

$$x_1 < x_2 < y_1 < x_3 < y_2 < y_3 < x_4 < \cdots . \tag{A 3}$$

The hypothesis $p(x) = \tilde{p}(y)$ is tested by means of inversions. The number of inversions for y_i is defined as the number of values of x_j with $x_j < y_i$. There are two inversions for y_1 and three for y_2 in the example above.

Let Q denote the total number of inversions obtained by summation over all y_j. If $p(x) = \tilde{p}(y)$, Q is Gaussian distributed with the mean value (see Bronstein & Semendjajew 1991)

$$\langle Q \rangle_{p=\tilde{p}} = \frac{mn}{2} \tag{A 4}$$

and, for $n, m > 25$, with the standard deviation

$$\sigma(m, n) = \sqrt{\frac{nm(n+m+1)}{12}}. \tag{A 5}$$

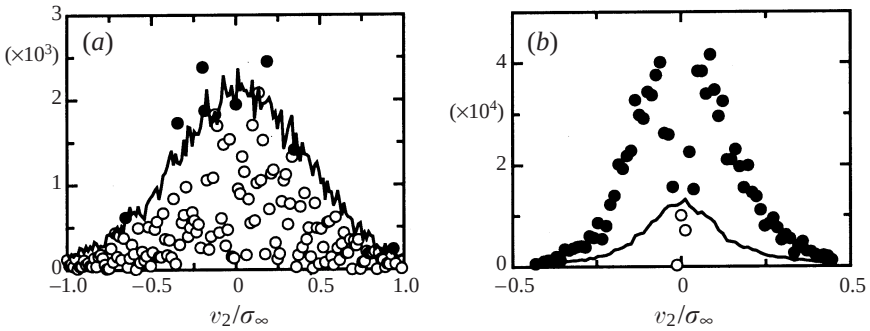

FIGURE 20. The quantities q (open and full circles) and $q_{\alpha=0.05}$ (solid lines) as functions of v_2 for different sets of length scales (v_3 is chosen to be zero). Full symbols indicate values of v_2 with $q > q_\alpha$. (*a*) $r_1 = L/2$ and $\Delta r = r_3 - r_2 = r_2 - r_1 = 2\lambda$. (*b*) $r_1 = L/2$ and $\Delta r = r_3 - r_2 = r_2 - r_1 = \lambda/4$.

Deviations from the expectation value (A 4) are usually measured by the absolute value of the difference $Q - \langle Q \rangle_{p=\tilde{p}}$:

$$q = |Q - \langle Q \rangle_{p=\tilde{p}}| = q(v_2, v_3, r_1, r_2, r_3). \tag{A 6}$$

The hypothesis will only be accepted if the measured value of q is smaller than a certain bound. This bound is determined by the so-called level of significance α and is usually denoted by q_α. For a given level α, q_α is chosen in such a way that the probability of measuring a value of q larger than the bound q_α is equal to α. In other words: even if $p(x) = \tilde{p}(y)$ holds, there is still a probability of α of measuring a value of q larger than q_α.

As q is the absolute value of a Gaussian-distributed random variable with a standard deviation given by equation (A 5), the bound q_α can easily be calculated from the inverse Gaussian error function (for details see Bronstein & Semendjajew 1991).

The test described above has to be performed for a large number of parameters. According to the definitions (A 1) of x and y, q is a function of the velocity increments v_2 and v_3 and the length scales r_1, r_2, and r_3. In order to reduce the number of parameters, we choose v_3 to be zero and the differences $r_3 - r_2$ and $r_2 - r_1$ to be equal: $\Delta r = r_3 - r_2 = r_2 - r_1$.

Figure 20(*a*) shows the quantities q and $q_{\alpha=0.05}$ as functions of v_2 for rather large scales, where we expect the Markov condition to be fulfilled: $r_1 = L/2$ and $\Delta r = 2\lambda$. In fact, for only eight out of 163 values of v_2 (i.e. 5%), q is larger than the bound q_α. We may therefore accept the hypothesis for the chosen set of length scales.

A different behaviour is obtained for small values of Δr. In figure 20(*b*), q and $q_{\alpha=0.05}$ are plotted for $r_1 = L/2$ and $\Delta r = \lambda/4$. The plot confirms what was suggested by figure 11. For almost all values of v_2, q is larger than q_α. Consequently, equation (A 2) is violated.

A quantitative measure for the validity of the hypothesis which is easier to handle is the expectation value of the quantity t, where t is defined as follows:

$$t = \frac{q}{\sigma(m,n)} = \frac{|Q - \frac{1}{2}mn|}{\sigma(m,n)} \tag{A 7}$$

(σ is the expected standard deviation of q, see equation (A 5)). If the hypothesis holds, t is the absolute value of a Gaussian-distributed random variable with mean value zero and standard deviation one. The expectation value $\langle t \rangle$ of t, where averaging is

done with respect to v_2, should therefore be $\sqrt{2/\pi} \approx 0.8$. Values of $\langle t \rangle$ larger than $\sqrt{2/\pi}$ indicate that equation (5.2) is violated.

Appendix B. An estimation of the influence of the fourth-order Kramers–Moyal coefficient

A quantitative measure for the importance of the influence of higher-order Kramers–Moyal coefficients can be obtained by estimating the influence of the fourth-order coefficient D_4 on the evolution of the eighth-order structure function. Equation (4.11) for $n = 8$ is given by (5.9). In particular, we will look for a lower bound of T_2 and an upper bound of T_4. With the results obtained for D_2 (see § 5.2), $T_2(r)$ can be written as

$$\begin{aligned} T_2(r) &= 8 \times 7 \int_{-\infty}^{+\infty} v^6 D_2(v,r)\, p(v,r)\, \mathrm{d}v \\ &= 8 \times 7 \int_{-\infty}^{+\infty} v^6 (\alpha(r) - \delta(r)v + \beta(r)v^2)\, p(v,r)\, \mathrm{d}v \\ &= 8 \times 7 \{\alpha(r)\langle v(r)^6 \rangle - \delta(r)\langle v(r)^7 \rangle + \beta(r)\langle v(r)^8 \rangle\}. \end{aligned} \tag{B 1}$$

The seventh-order moment $\langle v(r)^7 \rangle$ is negative in the inertial range; therefore, we can take as a lower bound for $T_2(r)$

$$T_2(r) \geqslant 8 \times 7\alpha(r)\langle v(r)^6 \rangle = T_2^{lb}(r). \tag{B 2}$$

$T_4(r)$ can be written as

$$\begin{aligned} T_4(r) &= 8 \times 7 \times 6 \times 5 \int_{-\infty}^{+\infty} v^4 (c_0(r) - c_1(r)v + c_2(r)v^2)\, p(v,r)\, \mathrm{d}v \\ &= 8 \times 7 \times 6 \times 5 \{c_0(r)\langle v(r)^4 \rangle - c_1(r)\langle v(r)^5 \rangle + c_2(r)\langle v(r)^6 \rangle\}. \end{aligned}$$

$\langle v(r)^5 \rangle$ is negative in the inertial range, the term $-c_1(r)\langle v(r)^5 \rangle$ is therefore positive. Throughout the inertial range, the moments of the absolute values of the velocity increment fulfil the relation

$$\langle |v(r)|^n \rangle \leqslant \langle |v(r)|^{n+1} \rangle. \tag{B 3}$$

Thus, we obtain as an upper bound for T_4

$$T_4(r) \leqslant 8 \times 7 \times 6 \times 5 \{c_0(r) + c_1(r) + c_2(r)\} \langle v(r)^6 \rangle = T_4^{ub}(r). \tag{B 4}$$

Equations (B 4) and (B 2) enable us to estimate the ratio $T_4(r)/T_2(r)$:

$$\frac{T_4(r)}{T_2(r)} \leqslant \frac{T_4^{ub}(r)}{T_2^{lb}(r)} = \frac{6 \times 5(c_0(r) + c_1(r) + c_2(r))}{\alpha(r)} = X(r). \tag{B 5}$$

When estimating the lower bound for T_2, we neglected the term containing the eighth-order structure function (see equation (B 1)). The actual value of the ratio $T_4(r)/T_2(r)$ is therefore much smaller than the quantity $X(r)$ defined above.

Appendix C. The equation for the moments of the absolute value of the velocity increment

For the sake of simplicity, the following case will be considered:

$$\left.\begin{aligned} D_1(v,r) &= -\gamma(r)v, \\ D_2(v,r) &= \alpha(r) - \delta(r)v + \beta(r)v^2. \end{aligned}\right\} \tag{C 1}$$

(Preliminary results on other data sets indicate that the nonlinear terms in D_1 can be neglected for high Reynolds numbers ($Re_\lambda \geqslant 1000$).) The Fokker–Planck equation (4.9) with the coefficients (C 1) reads

$$-r\frac{\partial}{\partial r}p(v,r) = \frac{\partial}{\partial v}\{\gamma v p(v,r)\} + \frac{\partial^2}{\partial v^2}\{(\alpha - \delta v + \beta v^2)\, p(v,r)\}. \tag{C 2}$$

By changing the sign of v, the equation for $p(-v,r)$ can be obtained:

$$-r\frac{\partial}{\partial r}p(-v,r) = \frac{\partial}{\partial v}\{\gamma v p(-v,r)\} + \frac{\partial^2}{\partial v^2}\{(\alpha + \delta v + \beta v^2)\, p(-v,r)\}. \tag{C 3}$$

The equations for $p(v,r)$ and $p(-v,r)$ differ due to the linear term δ in D_2. In general, any even-order term in D_1 and any odd-order term in D_2 will cause a difference in those equations. Let $S_v^n(r)$ denote the velocity structure function of order n and $T_v^n(r)$ the corresponding structure function of the absolute value of the velocity increment. In terms of the probability densities $p(v,r)$ and $p(-v,r)$, the structure functions $S_v^n(r)$ and $T_v^n(r)$ read

$$\left.\begin{aligned} S_v^n(r) &= \langle v(r)^n \rangle = \int_{-\infty}^{+\infty} v^n p(v,r)\,\mathrm{d}v, \\ T_v^n(r) &= \langle |v(r)|^n \rangle = \int_0^{+\infty} v^n \{p(v,r) + p(-v,r)\}\,\mathrm{d}v, \\ t_v^n(r) &= \int_0^{+\infty} v^n \{p(v,r) - p(-v,r)\}\,\mathrm{d}v. \end{aligned}\right\} \tag{C 4}$$

The definition of the functions $t_v^n(r)$ will prove to be convenient for the following calculation. Inserting equations (C 2) and (C 3) into (C 4), it is possible to derive a hierarchy of differential equations for $S_v^n(r)$ and $T_v^n(r)$:

$$\left.\begin{aligned} r\frac{\partial}{\partial r}S_v^n(r) &= n\{\gamma(r) - (n-1)\beta(r)\}S_v^n(r) \\ &\quad -n(n-1)\alpha(r)S_v^{n-2}(r) + n(n-1)\delta(r)S_v^{n-1}(r), \\ r\frac{\partial}{\partial r}T_v^n(r) &= n\{\gamma(r) - (n-1)\beta(r)\}T_v^n(r) \\ &\quad -n(n-1)\alpha(r)T_v^{n-2}(r) + n(n-1)\delta(r)t_v^{n-1}(r). \end{aligned}\right\} \tag{C 5}$$

Equations (C 5) are valid for $n \geqslant 2$ and if the p.d.f.(s) fulfil the following conditions: for $v \to \infty$, $p(v,r)$ decays faster than any power of v, for $v = 0$ the slope of $p(v,r)$ is finite.

The equations for odd order exhibit fundamental differences. The terms containing δ incorporate for S^n a large even moment S^{n-1}, while the integral t^{n-1}, incorporated for T^n, is small. Furthermore, the term depending on S^{n-2} vanishes for $n = 3$, whereas T^1 has a non-zero value.

The latter statement is remarkable. The equations for S^3 and T^3 not only differ due to the coefficient δ, as might be expected from equations (C 2) and (C 3), but also due to the constant term α in D_2. While δ is a rather small quantity with large experimental errors (see § 5.4), α is experimentally well-defined (see § 6). The difference between the equations for T^3 and S^3 can therefore by no means be regarded as negligible. As, in general, the equation for T^n depends on T^{n-2} (see equation (C 5)), the difference between T^3 and S^3 will lead to differences between T^n and S^n for each odd-order moment.

As a last remark, we want to point out that higher-order terms in equation (C 1), as indicated experimentally in equation (5.6), lead to a set of equations for the

moments which are not closed, i.e. the equation for the nth-order moment depends on higher-order moments.

REFERENCES

Amblard, P.-O. & Brossier, J.-M. 1999 On the cascade in fully developed turbulence. The propagator approach versus the Markovian description. *Eur. Phys. J.* B **12**, 579.

Arneodo, A., Baudet, C., Belin, F. *et al.* 1996 Structure functions in turbulence, in various flow configurations, at Reynolds number between 30 and 5000, using extended self-similarity. *Europhys. Lett.* **34**, 411.

Aronson, D. & Löfdahl, L. 1993 The plane wake of a cylinder. Measurements and inferences on the turbulence modelling. *Phys. Fluids* A **5**, 1433.

Benzi, R., Ciliberto, S., Baudet, C. *et al.* 1993 Extended self-similarity in the dissipation range of fully developed turbulence. *Europhys. Lett.* **24**, 275.

Bronstein, I. N. & Semendjajew, K. A. 1991 *Taschenbuch der Mathematik*. Teubner, Stuttgart.

Castaing, B., Gagne, Y. & Hopfinger, E. J. 1990 Velocity probability density functions of high Reynolds number turbulence. *Physica* D **46**, 177.

Chabaud, B., Naert, A., Peinke, J., Chilla, F., Castaing, B. & Hebral, B. 1994 A transition toward developed turbulence. *Phys. Rev. Lett.* **73**, 227.

Chilla, F., Peinke, J. & Castaing, B. 1996 Multiplicative Processes in turbulent velocity statistics: A simple analysis. *J. Phys. II Paris* **5**, 455.

Cleve, J. & Greiner, M. 2000 The Markovian methamorphosis of a simple turbulent cascade model. *Phys. Lett.* A **273**, 104.

Davoudi, J. & Tabar, M. R. 1999 Theoretical model of the Kramers–Moyal description of turbulence cascades. *Phys. Rev. Lett.* **82**, 1680.

Davoudi, J. & Tabar, M. R. 2000 Multi-scale correlation functions in strong turbulence. *Phys. Rev.* E **61**, 6563.

Donkov, A. A., Donkov, A. D. & Grancharov, E. I. 1998 The exact solutions of one Fokker–Planck type equation used by R. Friedrich and J. Peinke in the stochastic model of a turbulent cascade. Preprint math-ph/9807010.

Dubrulle, B. 2000 Affine turbulence. *Eur. Phys. J.* B **13**, 1.

Fairhall, A. L., Dhruva, B., L'vov, V., Procaccia, I. & Sreenivasan, K. R. 1997 Fusion rules in Navier Stokes turbulence: First experimental tests. *Phys. Rev. Lett.* **79**, 3147.

Friedrich, R., Galla, T., Naert, A., Peinke, J. & Schimmel, T. 1998*a* Disordered structures analyzed by the theory of Markov processes. In *A Perspective Look at Nonlinear Media.* Springer.

Friedrich, R. & Peinke, J. 1997 Description of the turbulent cascade by a Fokker–Planck equation. *Physica* D **102**, 147.

Friedrich, R., Peinke, J. & Renner, Ch. 2000*a* How to quantify deterministic and random influences on the statistics of the foreign exchange market. *Phys. Rev. Lett.* **84**, 5224.

Friedrich, R., Siegert, S., Peinke, J. *et al.* 2000*b* Extracting model equations from experimental data. *Phys. Lett.* A **271**, 217.

Friedrich, R., Zeller, J. & Peinke, J. 1998*b* A note on the three-point statistics of velocity increments in turbulence. *Europhys. Lett.* **41**, 143.

Frisch, U. 1995 *Turbulence.* Cambridge University Press.

Ghashghaie, S., Breymann, W., Peinke, J., Talkner, P. & Dodge, Y. 1996 Turbulent cascades in foreign exchange markets. *Nature* **381**, 767.

Hänggi, P. & Thomas, H. 1982 Stochastic processes: Time evolution, symmetries and linear response *Phys. Rep.* **88**, 207.

Hatakeyama, N. & Kambe, T. 1997 Statistical laws of random strained vortices in turbulence. *Phys. Rev. Lett.* **79**, 1257.

Jimenez, J. & Wray, A. A. 1998 On the characteristics of vortex filaments in isotropic turbulence. *J. Fluid. Mech.* **373**, 255.

Kolmogorov, A. N. 1941 The local structure of turbulence in an incompressible viscous fluid for very high Reynolds number. *Dokl. Akad. Nauk. SSSR* **30**, 301.

Kolmogorov, A. N. 1962 A refinement of previous hypotheses concerning the local structure of turbulence in a viscous incompressible fluid at high Reynolds number. *J. Fluid Mech.* **13**, 82.

Landau, L. D. & Lifschitz, E. M. 1987 *Fluid Mechanics*, 2nd Edn. Pergamon.

Lück, St., Peinke, J. & Friedrich, R. 1999 A uniform statistical description of the transition between near and far field turbulence in a wake flow. *Phys. Rev. Lett.* **83** (26), 5495.

L'vov, V. & Procaccia, I. 1996 Fusion rules in turbulent systems with flux equilibrium. *Phys. Rev. Lett.* **76**, 2898.

Marcq, P. & Naert, A. 1998 A Langevin equation for the energy cascade in fully developed turbulence. *Physica* D **124**, 368.

Monin, A. S. & Yaglom, A. M. 1975 *Statistical Fluid Mechanics.* MIT Press.

Naert, A. 1995 Turbulence dans un jet d'helium gazeux a basse temperature. PhD thesis, Grenoble.

Naert, A., Friedrich, R. & Peinke, J. 1997 A Fokker–Planck equation for the energy cascade in turbulence. *Phys. Rev.* E **56**, 6719.

Nelkin, M. & Stolovitzky, G. 1996 Limitations of random multipliers in describing turbulent energy dissipation. *Phys. Rev.* E **54**, 5100.

Obukhov, A. M. 1962 Some specific features of atmospheric turbulence. *J. Fluid Mech.* **13**, 77.

Pedrizzetti, G. & Novikov, E. A. 1994 On Markov modelling of turbulence. *J. Fluid Mech.* **280**, 69.

Pedrizzetti, G., Novikov, E. A. & Praskovsky, A. 1996 Self-similarity and probability distributions of turbulent intermittency. *Phys. Rev.* E **53**, 475.

Peinke, J., Castaing, B., Chabaud, B., Chilla, F., Hebral, B. & Naert, A. 1994 On a fractal and experimental approach to turbulence. In *Fractals in the Natural and Applied Sciences*, p. 295. Elsevier.

Peinke, J., Klein, M., Kittel, A., Okninsky, A., Parisi, J. & Roessler, O. E. 1993 On chaos, fractals and turbulence. *Physica Scripta* **T49**, 672.

Polyakov, A. M. 1995 Turbulence without pressure. *Phys. Rev.* E **52**, 6183.

Rajaratnam, N. 1976 *Turbulent Jets.* Elsevier.

Reisner, B., Renner, Ch., Lück, S., Peinke, J., Chilla, F. & Friedrich, R. 1999 A new method to characterize inhomogeneous turbulence. In *Fundamental Problematic Issues in Turbulence*, p. 361. Birkhäuser.

Risken, H. 1984 *The Fokker–Planck Equation.* Springer.

Sreenivasan, K. R. & Antonia, R. A. 1997 The phenomenology of small-scale turbulence. *Ann. Rev. Fluid Mech.* **29**, 435.

Takahashi, N., Kambe, T., Nakano, T., Gotoh, T. & Yamamoto, K. 1999 Probability density function of longitudinal velocity increment in homogeneous turbulence. *J. Phys. Soc. Japan* **68**, 86.

Yakhot, V. 1998 Probability density and scaling exponents of the moments of longitudinal velocity difference in strong turbulence. *Phys. Rev.* E **57**, 1737.